

Some Aspects on Geometric and Matrix Work-hardening Characteristics of Sintered Cold Forged Copper Alloy Preforms

Rajeshkannan A^{a*}, Devi S Rengamani^b, Alok Sharma^{c,d}

^aDepartment of Mechanical Engineering, School of Engineering & Physics, Faculty of Science, Technology & Environment, The University of the South Pacific – USP, Laucala Campus, Suva, Fiji

^bAyya Nadar Janaki Ammal College, Sivakasi, Tamil Nadu, India

^cDepartment of Electrical & Electronics Engineering, School of Engineering & Physics, Faculty of Science, Technology & Environment – USP, Laucala Campus, PMB, Suva, Fiji

^dInstitute for Integrated and Intelligent Systems, Griffith University, Australia

Received: February 18, 2013; Revised: September 9, 2013

Powder metallurgy (P/M) material subjected to plastic deformation results into densification, however the extended deformation would not only enhance the densification also supplements the strain hardening. Unlike fully dense material that would only undergo strain hardening while plastic deformation, the P/M material leads to pore closure as well; this phenomenon complicates the work hardening mechanism. The present study revealed that both strain and density configures strengthening of P/M preform, which respectively termed as matrix and geometric work hardening. An attempt has been made to delineate some aspects of work hardening behaviour with the influence of different aspect ratios of sintered and cold deformed copper alloy preforms. The preforms were initially prepared through conventional P/M route and finally subjected to cold upsetting under dry friction condition. A statistical analysis has also been introduced to study the quantitative impact of strain and density in the presence of aspect ratio on work hardening rate characteristics.

Keywords: work hardening, relative density, axial strain, aspect ratios

1. Introduction

Cold forging on sintered powder preforms would undergo both ductile fracture and strain hardening mechanisms, which in particular demonstrate the feasibility of forming processes. These mechanisms subsequently results in promoting densification and mechanical properties in the final products^{1,2}. In general, ductile fracture is the common mode of failure when material is subjected to plastic deformation³; this however is an obscured phenomenon as it depends on many other parameters. For P/M materials, the factors can be broadly categorized into initial powder characteristics, process parameters, operating parameters and material parameters. A comprehensive review on ductile fracture in metal forming has been given by Alexandrov and Lyamina⁴. Ductile fracture of materials is a consequence of void nucleation, growth and coalescence⁵, in case of porous materials it is readily available so the extensive deformation results into void closure or fracture at free surfaces⁶. A ductile fracture model has been established using the modified Rice and Tracey approach by Straffelini and Fontanari for a plain carbon and an alloy or high strength steel. It was observed that the model was predicting the fracture criteria better for plain carbon steel as compared to the alloy steel. It is due to the microstructural heterogeneity of the alloy that overestimates the experimental equivalent fracture strains⁷. The shape of porosities that present in the P/M preform governs and complicates the fracture criteria as it may not possess a regular geometry at every instant.

Using the self-consistent method, a ductile fracture criterion has been established by assuming the porosities shapes as a combination of spherical, cylindrical or disk. In which, voids are considered explicitly to propose a void coalescence criterion and is further considered as a homogenized continuum for porous plasticity models. The calibrated computational model is reported to successfully predict crack extension in various fracture specimens⁸.

Satsangi et al. proposed an elastic – plastic finite element method to analyze strain hardening phenomenon of porous material, when it is subjected to cold deformation in an incremental step. The variation of material parameters with relative density is also accounted to establish this model⁹. Strain hardening is the consequence of plastic deformation of the material that can be expressed in mathematical form using Ludwik equation¹⁰. The constants in this equation termed as K and n refer to strength coefficient and hardening exponent due to strain respectively. The aforementioned phenomenon supplements complexity in P/M material due to explicit porosities associated with it. The closure of pores under extended deformation could be in the form of ductile fracture and subsequently enhance densification along with promoting strain hardening. It was found that strain hardening could happen in the P/M material by means of matrix as well as geometric¹¹; various attempts had been made to explain this behavior with different compositions, preform geometries and friction conditions as major influencing parameter¹²⁻¹⁶. However there were no attempt made to identify or rationalize how and when

*e-mail: ananthanarayanan_r@usp.ac.fj

geometric and/or matrix strain hardening is happening, as well as the level of contribution by each factor in the deforming preforms. In the present investigation an attempt has been made to rationalize this behaviour by considering copper alloy preform subjected to secondary deformation such as cold upsetting under dry friction condition. An empirical model has been suggested for work-hardening due to strain and densification. Using this model, the work hardening rate characteristics has also been explained. Finally, using statistical analysis the contribution of material parameters such as relative density and axial strain with the influence of various aspect ratios on work hardening rate has been quantified.

2. Experimental Details

2.1. Materials and characteristics

Electrolytic copper powder of less than 150 μm was procured and analysed for its purity, which was found to be 99.7% and the rest were insoluble impurities. The atomized aluminium powder and silicon powder of less than 37 μm size were also analyzed for its purity, which were found to be 99.93% and 99.90% respectively. All the aforementioned powders were obtained from M/S. Metal Powder Company, Thirumangalam, Madurai, Tamil Nadu, India.

2.2. Powder blending and compaction

The required amount of powders corresponding to C64200 that is Cu-7%Al-1.8%Si were measured and blended in a pot mill along with porcelain balls of ratio 1:1 by weight for a period of 18 hours in order to obtain homogeneous mix. The powder blend was die compacted to yield preform of 26 mm diameter with 11 mm, 16 mm & 26 mm heights on a 0.6 MN hydraulic press using a suitable die set assembly. The initial preform densities were maintained in the range of 80 ± 1 percent theoretical by employing pressure in the range of 280 ± 10 MPa.

2.3. Ceramic coating, drying and sintering

These green compacts were thoroughly coated on all surfaces with indigenously developed ceramic coating in order to protect them against oxidation during sintering. This coat was allowed to dry for a period of 10 hours under room temperature conditions. Further, the compacts were recoated in the direction 90° to the earlier one. This second coat was allowed to dry under aforesaid condition for a further period of 10 hours. These ceramic-coated compacts were dried at 300°C for a period of 30 minutes in an alumina boat placed inside the electric muffle furnace. After the drying sequence was completed, the furnace temperature was raised to $810 \pm 10^\circ\text{C}$. At this temperature, the compacts were sintered for 100 minutes followed by furnace cooling.

2.4. Cold deformation and measurements

The sintered preforms were cleaned from the ceramic residue and machined to such a dimension to provide the preforms of initial heights to diameter ratio (aspect ratio) of 0.4, 0.60 and 1. These preforms were compressed between flat dies in 60 tons capacity hydraulic press at an

incremental loading step of 0.02MN. After each step of loading, measurements of height, diameters (contact and bulged) using digital vernier caliper and density by invoking Archimedian principle and examination of the barreled surface of cracks were made. The preforms were deformed under dry friction condition. The schematic view of before and after deformation of the preform is shown in Figure 1.

3. Results and Discussion

3.1. Work hardening characteristics

Figure 2 is drawn between flow stress and true axial strain to exhibit copper preforms deformation characteristic under the influence of three different aspect ratios. Apparently, the nature of characteristic is found to be similar as such increasing strain increases flow stress, however the proportion at which stress increases or behaves is different. Thus, a best curve fitting technique is applied, as a consequence a third order polynomial curve with regression co-efficient of almost unity is observed. This reveals that stress behaves against strain in three different mechanisms; at initial stage, this falls between nil strain to 0.06 strain, its stress respectively zero to 262 MPa, relatively peak rise in stress. This may due to an initial applied incremental

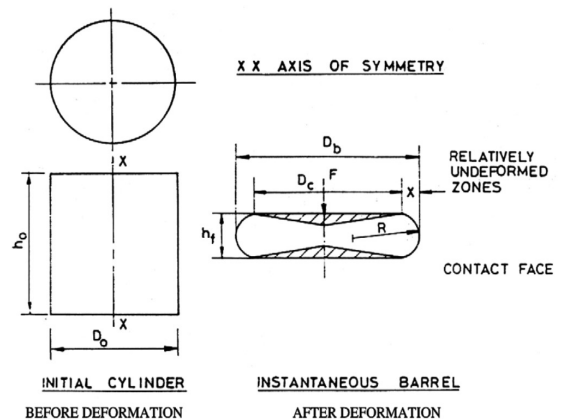


Figure 1. Schematic representation of the preform shape before and after deformation by upset forging.

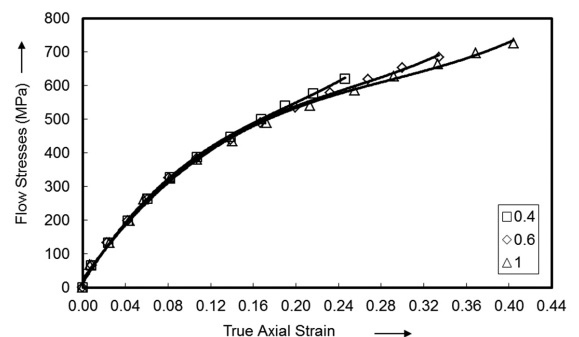


Figure 2. Characteristics of flow stress as a function of true axial strain.

load not bring sufficient enough to deform the specimen, as its initial pack density was around 80 percent theoretical and initial incremental loads were in the step of 2 tons. The second stage is between 0.06 strain and 0.14 strain, its respective stress fall between 262 MPa and 438 MPa. At this stage there is enough movement of particle, thus a mild retardation in rise of stress. The third stage, there is a continuous enhancement in stress till maximum density is attained or crack appears at free surface; although there is an enhancement in stress, at very slow rate, which predominantly contribute to matrix strain hardening in the specimen. Further observation reveals that lower aspect ratio exhibits higher stress compared to its counterpart; in other words, it can be concluded that decreasing the aspect ratio facilitates uniform deformation which results into quicker strain hardening.

An attempt has been made to relate flow stress as a function of density attained during deformation with the effect of aspect ratio in it, thus a plot has been drawn and is shown in Figure 3. Metal specimen subjected to cold plastic deformation results into jamming of grains and so to induce further deformation requires higher stresses, which is termed as matrix work hardening. This behavior is usual for ingot metallurgical products, whereas in powder metallurgical products, apart from a similar matrix strain hardening phenomena it also undergoes geometric work hardening phenomena. Thus, Figure 3 plays an important role to rationalize this concept; density rise, in other words closure of porosities leads to changes in effective volume of the preform, which is the consequence for geometric work hardening. It can be observed that despite density increment, flow stress also increases irrespective of aspect ratios, however a curve fitting technique is employed and it is found to be as third order polynomial with regression coefficient of unity. This helps to reveal its nature of characteristics to follow three different trend, respectively first stage between 0.8 and 0.82 relative density; second stage between 0.82 and 0.856 relative density and final stage from 0.856 to maximum density attained. The interesting point to note is that the first stage terminates at 262 MPa, and the second stage, although the stress value differs with aspect ratios, it can be approximated to 416 MPa flow stress. A very similar behavior has been observed in Figure 2 as well. Therefore, it can be firmly concluded that the copper alloy preform when subjected to cold upsetting, initially shows a peak rise in flow stress followed by a retardation in stress rise and finally there is an enhancement in flow stress but at very slow pace. Further observation proves that till stage 2, the influence of aspect ratios is negligible for all the practical considerations, in other words only at the final stage, the effect of preform geometry or aspect ratios are clearly evident. As opposed to Figure 2, Figure 3 exhibits that decreasing aspect ratio decreases the stress value for any given attained density, especially at the final stage. This is because higher effective volume requires higher load to deform and subsequently close the porosities, thus for any attained density higher aspect ratios needs higher load or stress to close its internal voids, which predominantly contributes to geometric work hardening behavior.

Figure 4 is drawn between stress and strain in log – log scale and Figure 5 is drawn between stress and density in semi-log scale in order to rationalize its mechanism into power law equation. Though the plots (Figures 2, 3) were drawn and characteristic natures have been established in third order polynomial form, it is difficult to control or understand behavior of stress with respect to the influencing parameter such as strain and density as it is influenced by four different constants. From Figure 4, the mathematical relationship can be obtained between stress and strain in plastic state that follows as;

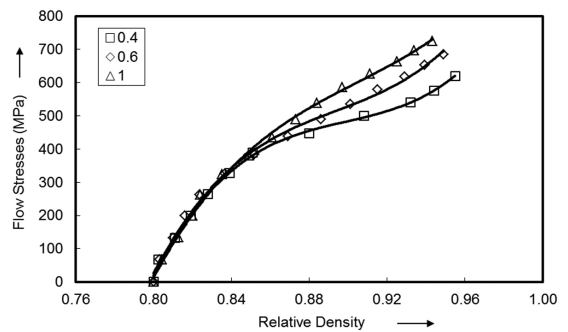


Figure 3. Characteristics of flow stress as a function of relative density.

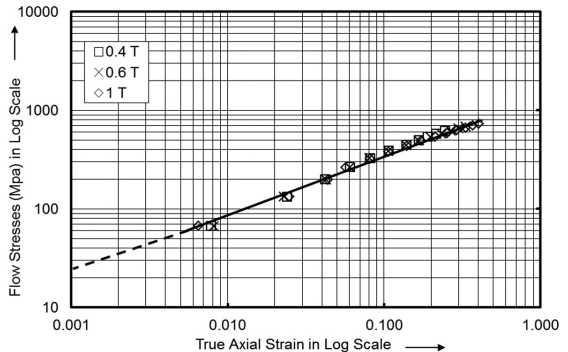


Figure 4. Characteristics of flow stress as a function of true axial strain in log-log scale.

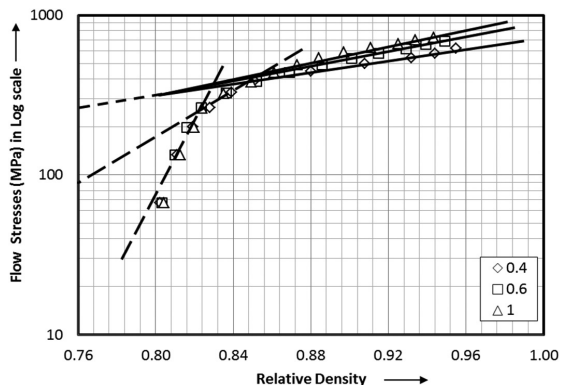


Figure 5. Characteristics of flow stress as a function of relative density in semi-log scale.

$$\sigma = K \epsilon^n \tag{1}$$

where, σ is flow stress; ϵ is true axial strain; K and n are strength coefficient and hardening exponent due to strain respectively. It was obtained that empirical constants, K and n were respectively found to be as 25 MPa and 0.59. Further interesting observation in Figure 4 is that invariably for all aspect ratio, flow stress follows single mechanism against strain, thus an empirical relationship can be established as, $\sigma = 25\epsilon^{0.59}$, for sintered copper alloy preforms. Therefore, it can be concluded that inducing axial strain the copper alloy preform gradually enhances the flow stress irrespective of preform geometry.

In Figure 5, flow stresses are in log scale whilst density is in ordinary scale since the density points are not much dispersed, therefore it's mathematical relationship can be formulated in a following manner;

A straight line equation can be formed from Figure 5 as

$$\log \sigma = mR + \log C \tag{2}$$

Equation 2 can be rearranged as

$$\log(\sigma / C) = mR \tag{3}$$

taking exponential, e on both sides of Equation 3 and further reducing will yield as,

$$\sigma = Ce^{mR} \tag{4}$$

where, $R = (\rho_f / \rho_{th})$, R is density ratio; ρ_f is forged density; ρ_{th} is theoretical density of copper alloy; C and m are respectively strength coefficient and hardening exponent due to densification.

It can be observed in Figure 5 that initial relative density from 0.80 to 0.85, flow stress follows two different mechanisms; however the influence of aspect ratio is practically negligible. As it was observed that characteristically all the aspect ratios follow identical mechanism during these stages and its densification span is relatively smaller, this can be neglected for all practical purpose. Thus the interest is shown for third mechanism, where the trend is different for different aspect ratios and so it's empirical relationship follows as;

$$\sigma = 263e^{2.48R} \text{ for aspect ratio 1.0} \tag{5}$$

$$\sigma = 263e^{2.23R} \text{ for aspect ratio 0.6} \tag{6}$$

$$\sigma = 263e^{1.83R} \text{ for aspect ratio 0.4} \tag{7}$$

Although the value of C , for all aspect ratios remain constant, the slope, m differs. This clearly proves that smaller the 'm' value, slower the rate of resistance to deformation for a given relative density. In other words, increasing the aspect ratio in general increases the flow stress at any attained density in the copper alloy preforms.

3.2. Work hardening rate characteristics

An attempt was made to determine work hardening rate and establish its relationship as a function of true axial strain and relative density. Since the flow stress – true axial strain

established single mechanism; the relationship obtained is shown in Equation 1,

Now, differentiating Equation 1 with respect to strain, ϵ , gives as;

$$\frac{d\sigma}{d\epsilon} = Kne^{(n-1)\epsilon} \tag{8}$$

Reducing Equation 8, results into;

$$\frac{d\sigma}{d\epsilon} = \frac{n\sigma}{\epsilon} \tag{9}$$

where, n is empirical constant found to be 0.59, from Figure 2; and, $\frac{d\sigma}{d\epsilon}$ is work hardening rate.

Using Equation 9, the work hardening rate can be obtained for various strain values, and a plot is constructed between these two parameters including the effect of aspect ratios, which is shown in Figure 6. The characteristic nature follows a power law relationship, in other words it follows a 80:20 rule; meaning thereby 80% of effect is due to 20% of cause. During the initial stage, say from 0.00 to 0.14 true axial strains, copper alloy preform exhibits higher work hardening rate, however the span of strain inducement is relatively low. Further it is observed that the rate at which work hardening falls down is also high during this stage. This can be due to the material that consist relatively higher amount of porosities, hence unable to bear resistance against deformation. Yet, this can contribute to more for geometric work hardening than for matrix work hardening in the sintered PM preform. This behavior can be further be ascertained by observing a plot between work hardening rate and density shown in Figure 7. That is from 0.80 to around 0.83 relative densities, there is a drastic decrease in work hardening rate due to closure of pores during deformation. However in the later stage, that is after 0.14 strain till to the end, the effect of work hardening rate is found to be qualitatively 20% despite strain applied could be 80%. This reveals that very slow change in the work hardening rate occurs irrespective of aspect ratios with relatively large amount of strain induced. At this stage the work hardening is much due to matrix than geometric, which can further be proved by establishing relationship between work hardening rate and relative density shown in Figure 7. That is from 0.83 to approximately 0.96 relative densities (relatively 80%),

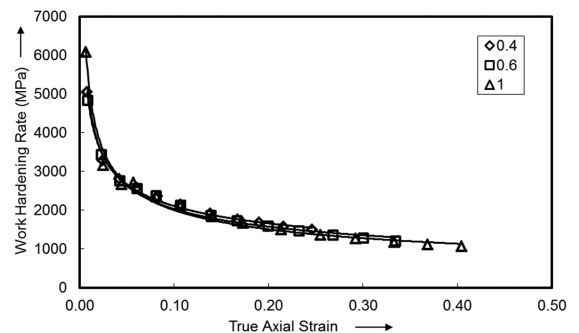


Figure 6. Characteristics of work hardening rate as a function of true axial strain.

the effect on work-hardening rate is very low (relatively 20%), this is due to gradual closure of pores. Since the pores closure are very gradual unlike in the first stage this reveals strain inducement is more uniform throughout the preform; particles as well as pores both move at equal pace in the direction of deformation resulting into pore closure as well as work hardening. This is the reason work hardening rate gradually decreases against relative density.

In order to establish the true behavior for work hardening rate against true axial strain and relative density, the parameters are expressed in log scale. Figure 8 is drawn between work hardening rate and true axial strain with influence of aspect ratio in log-log scale. It can be observed that there is practically nil influence by the aspect ratio, and a similar observation had been found in Figure 4. Although flow stress gradually increases over true strain (in Figure 4), the rate at which work hardening has been induced in the preform is decreasing due to continuous closure of pores or enhancement of density (Figures 7, 9). Figure 9 has been drawn between work hardening rate and relative density in semi-log scale. As observed in Figure 7, from 0.8 to 0.83 relative density range, the work hardening rate drastically reduces; in addition it is observed that there is a nil effect of aspect ratio during this stage. Although density is of short span, this reveals that more of hardening is due to geometric in nature. However, the later stage (0.83 to approximately 0.96 relative density) shows a gradual decrease in work hardening rate against density that ascertains hardening is

more due to matrix than geometric in nature. Further, it is observed that the lower the aspect ratio, higher the work hardening rate for any given relative density.

3.3. Work hardening rate – statistical analysis

Overall, it has been delineated that work hardening is due to strain induced and porosity closed or density enhanced, which in certain proportion add to matrix and geometric hardening. The statistical techniques can be used to identify the contribution of these two factors in the presence of three different aspect ratios. Thus analysis of variance (ANOVA) and F-test has been carried out in the experimental data. The four different random sampling variables has been chosen for relative density and axial strain of three different aspect ratios, however to represent the true behaviour of a lot, equally distributed values are opted. Megastat software has been used to carry out ANOVA exercise and the result of it is depicted in Table 1, 2.

The notations used in the tables are expressed and is explained elsewhere¹⁷

$$ss = \sum_{i=1}^n X_i \tag{10}$$

where, *ss* is sum of squares due to the total variation, *X_i* is value of considered parameter, *n* is the sample size.

$$df = n - 1 \tag{11}$$

$$MS = \frac{SS}{df} \tag{12}$$

where, *df* is the degrees of freedom, *MS* is mean square or variance and *F* is the Test-*F* value that can be calculated by, (*MS*/*MS_E*) where, *MS_E* is the mean square error.

Since the analysis was considered for a level of significance of 5%, the *F_α* value has been taken to 5%, this is a critical value obtained from *F* distribution table¹⁸. This value represents a level of confidence up to 95%. Observation of both the tables reveals that the ‘*F* value’ found to be greater than ‘*F_α* value’, which confirms that the considered variables are of statistical and physical significance. Generally, greater the *F* value is, the greater the effect on work hardening rate. The last column of these tables is the contribution of variables in percentage. It can be clearly observed that axial strain is greatly contributing to work-hardening rate with nil influence of aspect ratios.

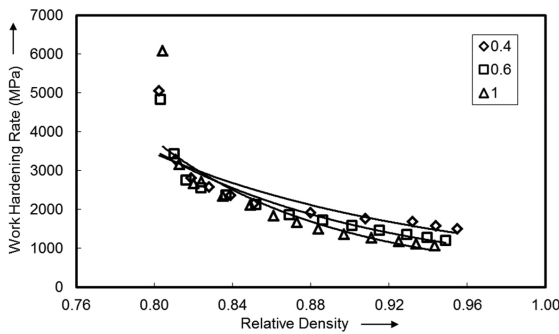


Figure 7. Characteristics of work hardening rate as a function of relative density.

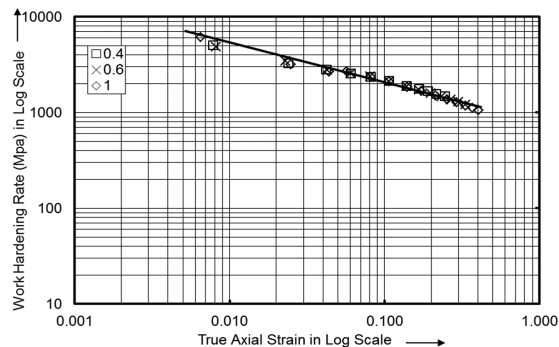


Figure 8. Characteristics of work hardening rate as a function of axial strain in log-log scale.

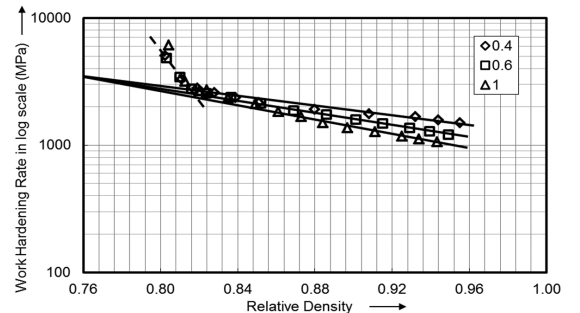


Figure 9. Characteristics of work hardening rate as a function of relative density in semi-log scale.

Table 1. Randomized ANOVA of aspect ratio and relative density on work hardening rate.

Parameter	SS	df	MS	F	$F_{\alpha=0.5\%}$	%C
Aspect Ratio	323,750.00	2	161,875.00	4.85	3.98	8.23
Relative Density	3,411,091.67	3	1,137,030.56	34.08	3.59	86.69
Error	200,183.33	6	33,363.89			5.09
Total	3,935,025.00	11				100.00

Table 2. Randomized ANOVA of aspect ratio and true axial strain on work hardening rate.

Parameter	SS	df	MS	F	$F_{\alpha=0.5\%}$	%C
Aspect Ratio	29,388.85	2	14,694.43	9.89	3.98	0.87
True Axial Strain	3,340,890.65	3	1,113,630.22	749.46	3.59	98.87
Error	8,915.49	6	1,485.91			0.26
Total	3,379,194.99	11				100.00

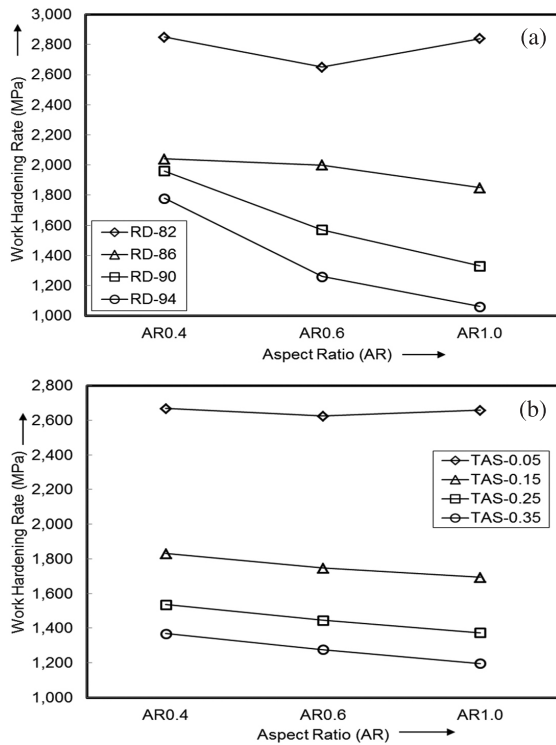


Figure 10. (a) Work hardening rate as a function of aspect ratio and relative density. (b) Work hardening rate as a function of aspect ratio and true axial strain (TAS).

On the other hand, though relative density is contributing significant amount for work hardening rate, there is an evidence of aspect ratio influence too. Further it is observed that there is a little amount of error contribution which is due to the interaction and noise effect.

The effect of aspect ratios along with relative density and axial strain on work-hardening rate has been shown in Figure 10a, b, which has been obtained from statistical analysis. General observation of these figures reveals that irrespective of variables considered such as density and strain, increasing aspect ratio decreases work hardening rate. This effect is particularly pronounced at higher strain and density range. However the rate of decrease in work hardening is relatively higher when density is considered comparing to axial strain.

4. Conclusions

The present investigation leads to the following major conclusions:

- Empirical relationship has been obtained for flow stress against strain and density, in which the effect of aspect ratio is also embedded. It was found that flow stress increases by increasing strain and density. However aspect ratio has nil impact when strain is considered; whereas against density, increasing aspect ratio increases flow stress.
- Overall, work-hardening rate decreases while increasing strain and density irrespective of aspect ratio considered, but at initial stage this effect is quite drastic followed by a very gradual decrease. Therefore, it is found that initial stage of deformation and densification are much contributed towards geometric work-hardening, whilst later stage is much for matrix work-hardening;
- Statistical analysis revealed the significance of material parameter such as strain induced and density attained on work-hardening rate, as well as the level of contribution by each parameter in percentage.

References

1. Narayanasamy R, Anandakrishnan V and Pandey KS. Effect of carbon content on instantaneous strain-hardening behavior of powder metallurgy steels. *Materials Science and Engineering A*. 2008; 497:505-511. <http://dx.doi.org/10.1016/j.msea.2008.07.053>
2. Chandramouli R, Kandavel TK, Shanmugasundaram D and Ashokkumar T. Deformation, densification and corrosion studies of sintered powder metallurgy plain carbon steel preforms. *Materials & Design*. 2007; 28(7):2260-2264. <http://dx.doi.org/10.1016/j.matdes.2006.05.018>
3. Xue L. Constitutive modeling of void shearing effect in ductile fracture of porous materials. *Engineering Fracture Mechanics*. 2008; 75(11):3343-3366. <http://dx.doi.org/10.1016/j.engfracmech.2007.07.022>
4. Alexandrov S and Lyamina E. Ductile fracture in metal forming: a review of selected issues. *Key Engineering Materials*. 2012; 528:1-11. <http://dx.doi.org/10.4028/www.scientific.net/KEM.528.1>
5. Kim J, Zhang G and Gao X. Modeling of ductile fracture: application of the mechanism based concepts. *International Journal of Solids and Structures*. 2007; 44(6):1844-1862. <http://dx.doi.org/10.1016/j.ijssolstr.2006.08.028>
6. Rajeshkannan A, Pandey KS, Shanmugam S, Narayanasamy R and Narayan S. Some studies on sintered cold deformed plain carbon alloy steels. *Materials & Design*. 2012; 33:115-120. <http://dx.doi.org/10.1016/j.matdes.2011.07.020>
7. Straffelini G and Fontanari V. Stress state dependent fracture behavior of porous PM steels. *Engineering Fracture Mechanics*. 2011; 78(6):1067-1076. <http://dx.doi.org/10.1016/j.engfracmech.2010.12.009>
8. Bompard Ph, Wei D, Guennouni G and Francois D. Mechanical and fracture behaviour of porous materials. *Engineering Fracture Mechanics*. 1987; 28(5-6):627-642. [http://dx.doi.org/10.1016/0013-7944\(87\)90058-0](http://dx.doi.org/10.1016/0013-7944(87)90058-0)
9. Satsangi PS, Sharma PC and Prakash R. An elastic – plastic finite element method for the analysis of powder metal forging. *Journal of Materials Processing Technology*. 2003; 136(1-3):80-87. [http://dx.doi.org/10.1016/S0924-0136\(02\)00939-1](http://dx.doi.org/10.1016/S0924-0136(02)00939-1)
10. Lei S, Zhang JY, Niu JJ, Liu G, Zhang X and Sun J. Intrinsic size-controlled strain hardening behavior of nanolayered Cu/Zr micropillars. *Scripta Materialia*. 2012; 66(9):706-709. <http://dx.doi.org/10.1016/j.scriptamat.2011.12.032>
11. Narayanasamy R, Anandakrishnan V and Pandey KS. Effect of geometric work-hardening and matrix work-hardening on workability and densification of aluminium-3.5% alumina composite during cold upsetting. *Materials & Design*. 2008; 29(8):1582-1599. <http://dx.doi.org/10.1016/j.matdes.2007.11.006>
12. Venugopal P, Annamalai S, Jagannathan V and Venkatramani V. On the apparent strength-coefficient, strain-hardening exponent and boundary-friction coefficient of sintered P/M copper compacts. *Journal of Mechanical Working Technology*. 1987; 14(2):137-147. [http://dx.doi.org/10.1016/0378-3804\(87\)90056-8](http://dx.doi.org/10.1016/0378-3804(87)90056-8)
13. Rajeshkannan A and Narayan S. Strain hardening behaviour in sintered Fe-0.8%C-1.0%Si-0.8%Cu powder metallurgy preform during cold upsetting. *Proceedings of the Institution of Mechanical Engineers - Part B: Journal of Engineering Manufacture*. 2009; 223:1567-1574. <http://dx.doi.org/10.1243/09544054JEM1587>
14. Selvakumar N, Radha P, Narayanasamy R and Ganesan P. Neural network model for predicting strain hardening and densification constants of sintered aluminium performs. *Powder Metallurgy*. 2004; 47(3):261-266. <http://dx.doi.org/10.1179/003258904225020800>
15. Balakrishnan R and Thiyaagrajan S. A study of the flow properties of aluminium alloys. *Journal for Manufacturing Science and Production*. 2012; 12(2):81-86.
16. Selvakumar N, Mohan Raj AP and Narayanasamy R. Experimental investigation on workability and strain hardening behaviour of Fe-C-0.5Mn sintered composites. *Materials & Design*. 2012; 41:349-357. <http://dx.doi.org/10.1016/j.matdes.2012.04.053>
17. Montgomery DC, Runger GC, Hubele NF. *Engineering statistics*. 5th ed. Asia: Wiley; 2012. p. 285.
18. Walck C. *Handbook on statistical distributions for experimentalists*. 2007. p. 175. Available from: <http://www.stat.rice.edu/~dobelman/textfiles/DistributionsHandbook.pdf>. Access in: 01/07/2013.